Emergent electrochemistry in spin ice: Debye-Hückel theory and beyond

V. Kaiser,[1,2,3] J. Bloxsom,[4] L. Bovo,[4,5] S. T. Bramwell,[4] P. C. W. Holdsworth,[1] and R. Moessner[2]

[1]*Université de Lyon, ENS de Lyon, Université Claude Bernard, CNRS, Laboratoire de Physique, F-69342 Lyon, France*

[2]*Max-Planck-Institut für Physik komplexer Systeme, 01187 Dresden, Germany*

[3]*Center for Systems Biology Dresden, Max Planck Institute of Molecular Cell Biology and Genetics, 01307 Dresden, Germany*

[4]*London Centre for Nanotechnology and Department of Physics and Astronomy, University College London, London WC1H 0AH, United Kingdom*

[5]*Department of Innovation and Enterprise, University College London, 90 Tottenham Court Road, London W1T 4TJ, United Kingdom.*

(Received 7 March 2018; revised manuscript received 22 August 2018; published 9 October 2018)

We present a detailed theoretical and experimental study to show how a model system for the investigation of classic electrolyte theory emerges in a nonelectrical context. In particular we develop the thermodynamic treatment of spin ice as a "magnetolyte," a fluid of singly and doubly charged magnetic monopoles. This is equivalent to the electrochemical system $2H_2O = H_3O^+ + OH^- = H_4O^{2+} + O^{2-}$, but with perfect symmetry between oppositely charged ions. For this lattice magnetolyte, we present an analysis going beyond Debye-Hückel theory to include Bjerrum pairs. This is accurate at all temperatures and incorporates "Dirac strings" imposed by the microscopic ice rule constraints at the level of Pauling's approximation. Our theory is in close agreement with the specific heat from numerical simulations as well as new experimental measurements with an improved lattice correction, which we present here, on the spin ice materials $Ho_2Ti_2O_7$ and $Dy_2Ti_2O_7$. Our results provide new experimental tests of Debye-Hückel theory and its extensions and yield insights into the electrochemical behavior of water ice and liquid water, which are closely related to the spin ice magnetolyte.

DOI: 10.1103/PhysRevB.98.144413

I. INTRODUCTION

Capturing charge correlations in a Coulomb fluid is a notoriously challenging problem. Long-range interactions mean that the equilibrium state is only stabilized through the build up of charge screening correlations, so that approaches beyond simple perturbation theory are required, even at the highest temperatures and lowest charge concentrations. Debye and Hückel's [1] approximate solution of the problem, along with Bjerrum's extension [2] to include association, established a controlled theory that remains the cornerstone of theoretical approaches [3–5]. Comparatively recently, Fisher and Levin [6,7] extended the theory to cover the whole temperature-density phase diagram of a model fluid, while Kobelev *et al.* [8] treated lattice systems. Practically though, making contact with experiments in electrolytes, over a wide range of charge concentration, requires a more elaborate description, including the coupling between electrostatics and physicochemical effects. For example, Pitzer's model [9,10] is based on Debye-Hückel theory, but relies on several fitting parameters to include both solvation and steric effects.

More generally, the Debye-Hückel-Bjerrum paradigm is easily and commonly evaded in real systems: for example, its well-known exponential screening may give way to either oscillatory short-range decay [11,12] or anomalously long-ranged decay [13,14]. Such behavior is experimentally well defined, but at present poorly understood, suggesting the need to revisit the classic theories of electrolyte solutions [15].

Spin ice, a magnetic system, forms an unusual and unprecedented setting in which to investigate the foundations of electrochemistry. The starting point is a complex spin system with long-range dipolar interactions. The high lattice symmetry causes self-screening of the magnetic dipolar interactions between spins, which suppresses ferromagnetic or antiferromagnetic order and leads to the emergence of charge-carrying excitations ("magnetic monopoles") on a neutral background. The monopoles form a symmetric lattice Coulomb fluid, with monopole charges, in electrical units $\pm 0.009e$, $\pm 0.018e$ where $e = 1.602 \times 10^{-19}$ C is the elementary charge [16]. The relatively small value of the monopole charge compared to that of ions means that the Coulombic physics of spin ice asserts itself in the Kelvin temperature range [17].

While the magnetic monopoles of spin ice have generally been studied as a convenient route to analyzing magnetic properties, here we additionally emphasise the role of spin ice as a model electrochemical system. In particular we show how it broadens the scope of Coulomb systems to provide a model lattice Coulomb fluid whose thermodynamic properties are accessible to experiment over a broad temperature range that spans both the high and low temperature limits. Our result shows how Debye-Hückel theory *and its extensions* provide a very accurate description of this experimental system over the whole parameter range of interest. Spin ice in fact equates to an electrochemical system that is stripped of all the chemical complexity that generally complicates, and occasionally undermines, the Debye-Hückel approach. We argue that discovery of such a model system provides a valuable point of reference in electrochemistry, as it does in magnetism. In particular, future experiments could push beyond the regime of applicability of state-of-the-art theories, to provide new challenges in a controlled environment.

In general we treat spin ice as a "magnetolyte" rather than an "electrolyte." The difference is in part a change of units but, more importantly, a recognition of the fundamental differences between electricity and magnetism. Spin ice maps to water ice by associating spins (axial vectors) with proton displacements (polar vectors). The disordered yet highly correlated nature of these vector fields gives the Pauling entropy [18–20] and provides the effective ground state from which pointlike defects (magnetic monopoles and ionic defects, respectively) are thermally excited [21,22]. Essentially the same microscopic dipolar Hamiltonian with discrete symmetry applies to both cases [23] and from this emerges a $U(1)$ field with fractionalized [24,25], charge-carrying quasiparticle excitations that interact via the Coulomb potential.

In the case of spin ice the Coulomb interaction was exposed using the dumbbell model approximation [22] for dipolar spin ice [26], where the initial, complex problem was rewritten as a fluid of deconfined magnetic monopoles [22]. As the magnetic charges are induced, rather than free, their configurations and dynamics are constrained by a connected network of classical Dirac strings that carries the associated magnetic flux. This defines the magnetolyte. In the Pauling model of water ice, the ionic defects also carry induced charge and are connected by the equivalent of Dirac strings, but the axial versus polar vector nature of the problems (reflecting the absence or presence of fundamental charges, respectively) mean that the magnetolyte is perfectly symmetric, whereas the water ice electrolyte is not. In addition, water ice admits bonding or Bjerrum defects that are not relevant to spin ice. Beyond this, both the spin ice magnetolyte and water ice electrolyte differ from a primitive model electrolyte by the presence of the Dirac string network. However, this has less effect on the Debye-Hückel description than one might imagine. The reason is that the systems map approximately onto a generalized Coulomb fluid [27–29], where Poisson and non-Poisson fields fluctuate independently. However, for the detailed application of Debye-Hückel theory considered here, the Dirac string network needs to be properly accounted for.

Spin ice is particularly attractive as a model system as it naturally yields a Coulomb fluid in the grand canonical ensemble in which the external parameter is the chemical potential for monopole creation, rather than charge or fluid density. The thermodynamic constraints are therefore those of an electrochemical system that relaxes to chemical equilibrium in exact analogy with many electrolyte systems in a framework in which their numerical values can be estimated with precision. The perfect charge symmetry, due to the time reversal symmetry of magnetism, eliminates ion-specific effects, making it relatively easy to model. Furthermore, as the charges are quasiparticles confined to a solid state environment, pressure and volume are effectively decoupled from the Coulomb thermodynamics while the underlying lattice structure greatly facilitates entropy calculations. As a consequence we are able to adapt Debye-Hückel and association theory to the magnetolyte, allowing detailed comparison of theory both with simulation and with experiments on spin ice materials.

Debye-Hückel theory for spin ice was first formulated and tested in Ref. [30], but the theory developed there is only a rough approximation to spin ice, as reflected in significant differences between theory and experiment. The same deficiency occurs in another Debye-Hückel approach [31], although there the differences between theory and experiment were masked by parameter fitting. Here we develop a full thermodynamic description of the dumbbell model that allows a complete quantitative comparison of theory, experiment, and simulation. This goes beyond the original work [30] in three important ways. First, see Fig. 1(a), we take into account the fact that the monopole vacuum state is actually an ensemble of configurations of close packed and constrained magnetic moments with finite entropy density [18–20] that we include into the Coulomb fluid at the Pauling level of approximation [32]. This incorporates the fragmentation of the magnetic moments into a monopole and a vacuum contribution for arbitrary monopole concentrations [27]. By suppressing this contribution one recovers a simple lattice electrolyte [Fig. 1(b)] that is studied for comparison. Second [Fig. 1(c)], we allow for not only singly charged [30] but also doubly charged monopoles, in analogy with an electrochemical system of the form

$$2H_2O = H_3O^+ + OH^- = H_4O^{2+} + O^{2-}. \quad (1)$$

Considering double charges permits us to access the full temperature range (see Appendix B). Third [Fig. 1(d)], as well as formulating Debye-Hückel theory, we refine it through the systematic inclusion of neutral bound charge pairs for both the lattice electrolyte and the magnetolyte. This refinement is in the spirit of Bjerrum's theory, but is specifically adapted to the spin ice magnetolyte. The associated lattice electrolyte is treated using the technique of Ref. [8].

The net result of these developments may be assessed from either a magnetic perspective or an electrochemical one. In magnetic terms, we have an approximate, yet highly accurate, analytic solution of a three-dimensional spin model with long-range interactions—the dipolar spin ice model [26] (see below). Our solution approaches an exact description of dipolar spin ice over a restricted parameter range, where the Debye-Hückel linear approximation is valid. The parameters of the canonical spin ice materials $Ho_2Ti_2O_7$ (HTO) and $Dy_2Ti_2O_7$ (DTO) lie within this range at most temperatures; hence, as shown in Figs. 1(e) and 1(f), our theory describes their experimental and simulated specific heat with only very small systematic corrections (see Appendix A), showing that emergent quasiparticles stay a valid description over the full temperature range, well beyond their originally proposed region of validity. It should be noted that the experimental data of Figs. 1(e) and 1(f) improve on some previous measurements, in that hyperfine specific heat is accounted for and the nonmagnetic background component has been estimated with precision up to high temperature, allowing the close confrontation of experiment, theory, and simulation.

In electrochemical terms, the striking agreement between experiment, simulation, and theory shown in Figs. 1(e) and 1(f) confirms the existence of an emergent electrochemistry in spin ice over a full range of charge concentrations. To our knowledge a fully quantitative demonstration of the applicability of Debye-Hückel-Bjerrum theory to experimental specific heat measurements has not previously been achieved. Thus, the famous limiting law for the activity coefficient, which was discovered experimentally [33], before it was derived theoretically by Debye and Hückel [1] [see Eq. (15)], is implicit in our comparison of experiment and theory.

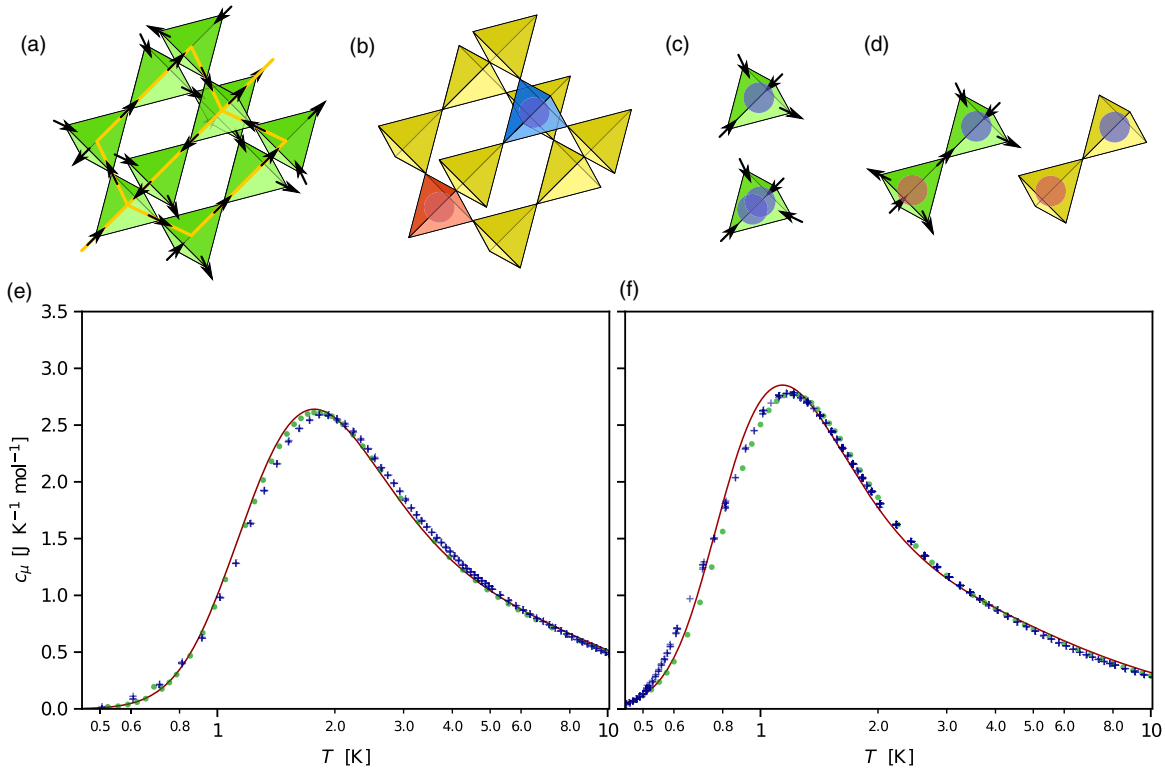

FIG. 1. Specific heat—experiment: A nonelectrical model system for Debye-Hückel theory and its extensions. The figure illustrates the monopole model of the magnetic system, spin ice, and theory versus experiment. (a) The spin ice state on the pyrochlore lattice forms a vacuum for magnetic monopoles in the magnetolyte model. (b) Neglecting the string network yields a diamond lattice electrolyte. (c) Magnetic monopoles of single charge (upper) and double charge (lower). (d) Charge pairs in the magnetolyte and electrolyte. (e) and (f) The experimental specific heat (blue crosses) of $Ho_2Ti_2O_7$ (e) and $Dy_2Ti_2O_7$ (f) as compared with simulations (green circles) and Debye-Hückel theory with monopole pairing included (red line).

However, going beyond this limit has proved difficult as a detailed comparison of theory and experiment for electrolytes has generally been hampered by imprecise knowledge of parameters, as well as the difficulty of accounting for strong correlations. In the case of the spin ice magnetolyte, the emergent nature and perfect symmetry of the magnetic charge largely eliminates these problems.

The models studied and developed in this paper, and tested numerically, are broadly relevant to a number of experimental systems in electrochemistry and magnetism. The lattice electrolyte model could essentially describe a weak (solid or liquid) electrolyte in which the dissociating ions are not strongly correlated with the "solvent." The magnetolyte model could, through the analogy between electro- and magnetostatics, describe water ice or, approximately, water itself. In these cases the solvent is correlated with the ions through Dirac strings or, equivalently, hydrogen-bonded chains. One result of our work is to show how such correlations may be factored into the Pauling entropy, to allow for a standard electrochemical description at the level of thermodynamics.

The remainder of the paper justifies our main result, Figs. 1(e) and 1(f), and exposes a number of other notable details. It is organized as follows. In the next section we develop the model magnetolyte, highlighting its specific characteristics compared to the lattice electrolyte. In Sec. III we present electrolyte and magnetolyte thermodynamics, developing equations of state within the Debye-Hückel approximation. The limits of the theory are given and extensions to it at low temperature, using a pair approximation, are discussed in Appendix D. In Sec. IV we test the theory by comparing specific data from both simulations and our new experiments. Conclusions are drawn in Sec. V.

II. MODELS: FROM ELECTROLYTE TO MAGNETOLYTE

Spin ice [18,19] is a corner sharing network of tetrahedra forming a pyrochlore lattice of localized, Ising-like magnetic moments, as shown in Fig. 1(a). The magnetic degrees of freedom transform, to an excellent approximation, into a fluid of magnetic monopoles [22] at the centers of the tetrahedra, forming a diamond lattice. The monopole charges emerge from flux lines, "Dirac strings," that connect the sites. The Dirac strings connect monopoles of opposite charge but they do not pair them in the sense of uniquely associating a given positive with a given negative charge: rather, they form a network whose nodes (the monopoles) are able to diffuse almost independently. The transformation is made by extending the spins into infinitesimally thin needles carrying net neutral dumbbells of charge that touch at the diamond lattice sites [22,34–36]. The total charge Q_α accumulated at the site $\alpha = 1, \ldots, N_0$, is the sum of the four dumbbell charges arriving at tetrahedron α. Allowed values are thus $Q_\alpha = 0, \pm Q, \pm 2Q$, where Q is the monopole charge, so that the Hamiltonian

reads

$$\mathcal{H} - \mathcal{H}_0 = \frac{1}{2}\sum_{\alpha\neq\beta}\frac{\mu_0 Q_\alpha Q_\beta}{4\pi r_{\alpha\beta}} - \mu N^i - \mu_2 N_2^i, \qquad (2)$$

with $r_{\alpha\beta}$ the distance separating sites α and β, and μ_0 the vacuum permeability. The chemical potentials μ and μ_2 are for single and double monopoles, N^i (N_2^i) are the respective number of (double) monopoles/charges for a given microstate, and $\mathcal{H}_0$ is the energy of the charge vacuum [22]. Strictly speaking, μ and μ_2 are excess terms [37], defined with respect to a reference state at $\mu = \mu_2 = 0$, which has random spin configurations constraining dense but globally charge neutral charge configurations. See Sec. III D for further discussion. Hence the complex magnetic problem maps to a lattice fluid of quasiparticles interacting via the Coulomb potential—a system identical to that of a neutral electrical fluid except that the charge Q_i is magnetic and the permittivity ϵ_0 is replaced by the inverse of the magnetic permeability $\frac{1}{\mu_0}$. In addition, we must include the constraint that the charges remain connected by the network of Dirac strings which captures the fact that the monopoles are induced, rather than free magnetic charge. The dielectric analog has deconfined polarization charges connected by a network of polarization loops, or strings carrying equivalent electrical flux. Indeed, in the absence of D/L defects the ice network can be thought of in exactly this manner [21].

The mapping to a grand canonical fluid means that the independent thermodynamic variables are T, μ, and μ_2, which together with the diamond lattice constant a and the monopole charge [22] completely specify the problem. In spin ice materials $\mu_2 = 4\mu$, but interesting physics can appear for other choices of this ratio [27]. Setting $\mu_2 = \infty$ imposes $N_2^i = 0$, which we define as the primitive model.

Neglecting the string network leads to a standard lattice electrolyte [30], while taking into account its additional features defines the magnetolyte system (which is equivalent to a description of water ice without D/L defects). In the absence of any charge, the Dirac string network carries a finite "Pauling" entropy [18,32], corresponding to the ensemble of spin configurations satisfying the ice rules with two spins pointing in and two out of each tetrahedron. It is accurately accounted for by the Pauling approximation $S_P \approx k_B N_0 \ln(\frac{3}{2})$ [32] providing a monopole vacuum with finite entropy. Configurations with a finite monopole concentration generally maintain some of this entropy, associated with the free space between the quasiparticles, so that each charge state should be supplemented with an entropic weight given by the number of spin microstates consistent with it. Certain microstates of the lattice electrolyte are forbidden by this procedure. For example, two adjacent $Q = 2$ charges cannot be nearest neighbors in the magnetolyte. These are high energy states and so not important in the fluid phase, but they can have consequences for monopole crystallization at high density [38]. In the following we are able to add this entropic weight at the mean-field level, which does not take such correlations into consideration.

A generic phase diagram for lattice electrolytes on bipartite structures allowing nonfrustrated ionic crystals has been studied in detail by Kobelev *et al.* [8], albeit for fields confined to lattice edges. For the primitive model, a fluid phase gives way to a crystalline phase via a transition that is either first or second order, separated by a tricritical point [39]. The magnetolyte with both single and double charges has a similar phase diagram, with crystallization to a double monopole zinc-blende structure [27,38,40]. The monopole-monopole interactions driving this evolution across the phase diagram can be parametrized by the interaction ratio $\zeta = \frac{u_a}{|\mu|}$, where $u_a = \frac{\mu_0 Q^2}{4\pi a}$ is the Coulomb energy scale for a nearest neighbor pair of charges. Monopole crystallization occurs for $\zeta = \frac{2}{\alpha} = 1.22$, where α is the Madelung constant for a diamond lattice [27], providing an upper bound for the stability of the fluid phase. For spin ice materials DTO and HTO, $\zeta = 0.71$ and $\zeta = 0.54$, respectively, placing them away from the phase boundary [41] yet far from the noninteracting limit.

The vacuum entropy implies that the idealized dumbbell model violates the third law of thermodynamics in that the entropy remains finite at the absolute zero of temperature. Experiments on both water ice [42,43] and spin ice [20] show a corresponding residual entropy. The spin systems of real spin ice materials are considered to be metastable [44] below some low temperature (estimated to be at least 0.3 K for spin ice), but in the temperature range considered in this paper they accurately approximate the dumbbell model at equilibrium, as our results confirm.

III. COULOMB FLUID THERMODYNAMICS

A. Grand potential

The electrolyte and magnetolyte free energies are of the form

$$\Omega = U_C - \mu N - \mu_2 N_2 - ST, \qquad (3)$$

where U_C, N, and N_2 are thermally averaged values for the Coulomb energy, the number of monopoles, and of double monopoles, respectively.

Following Ryzhkin [21], one can write an approximate expression for the vertex entropy of the magnetolyte by considering each type of vertex as a species of indistinguishable objects:

$$W = \left(\frac{1}{2}\right)^{2N_0}\frac{N_0!}{N_1!N_2!\cdots N_{16}!}, \qquad (4)$$

where N_a is the number of vertices of type $a = 1, \ldots, 16$. The prefactor $(1/2)^{2N_0}$ takes into account the compatibility of the spins shared between neighboring vertices.

Each vertex configuration corresponds to charge $0, \pm Q, \pm 2Q$, with six 2in-2out spin ice configurations corresponding to charge zero, four each of 3in-1out (and four 3out-1in) configurations corresponding to charge Q ($-Q$) and one all-in (all-out) vertex corresponding to charge $2Q$ ($-2Q$). For a system of $N = nN_0$ monopoles and $N_2 = n_2 N_0$ double monopoles in a system of N_0 sites one can hence set $N_1 = N_2 = \cdots N_6 = (1 - n - n_2)N_0/6$, $N_7 = N_8 = \cdots N_{14} = nN_0/8$, and $N_{15} = N_{16} = n_2 N_0/2$. It

follows that

$$S = -k_B N_0 \Big\{ n \ln\left(\frac{n}{2}\right) + n_2 \ln(2n_2) + (1-n-n_2)\ln(1-n-n_2) + (1-n-n_2)\ln\left(\frac{2}{3}\right)\Big\}. \tag{5}$$

This formula elegantly separates the entropy into a monopole term and a vacuum term: the last term approximates to the vacuum entropy and setting $n = n_2 = 0$ yields the Pauling entropy, $S_p = k_B N_0 \ln(3/2)$. The first three terms correspond to the entropy of a lattice gas with both single and double charges. Setting $n_2 = 0$ and excluding the vacuum entropy gives the primitive electrolyte entropy

$$S_e = -k_B N_0 [n \ln(n/2) + (1-n)\ln(1-n)], \tag{6}$$

used in [30]. For the double monopoles, the vertex weights modify their contribution compared to a free lattice gas, giving a contribution of $n_2 \ln(2n_2)$ rather than the $n_2 \ln(n_2/2)$ one might have expected. A final check can be made at high temperature, where one expects the single and double monopole concentrations to approach $n_\infty = \frac{1}{2}$ and $n_{2(\infty)} = \frac{1}{8}$, respectively. Plugging in these numbers yields the full entropy of $2N_0$ uncorrelated Ising degrees of freedom, $S_\infty = 2N_0 k_B \ln 2$.

Armed with this expression for the entropy we can find equations of state for the monopole fluid $n(\mu, \mu_2, T)$, $n_2(\mu, \mu_2, T)$ by minimizing Eq. (3) with respect to n and n_2:

$$n = \frac{\frac{4}{3}\exp(\beta\tilde{\mu})}{1 + \frac{1}{3}[4\exp(\beta\tilde{\mu}) + \exp(\beta\tilde{\mu}_2)]}, \qquad n_2 = \frac{\frac{1}{3}\exp(\beta\tilde{\mu}_2)}{1 + \frac{1}{3}[4\exp(\beta\tilde{\mu}) + \exp(\beta\tilde{\mu}_2)]}, \tag{7}$$

where

$$\tilde{\mu} = \mu - k_B T \ln(\gamma), \quad \tilde{\mu}_2 = \mu_2 - k_B T \ln(\gamma_2), \tag{8}$$

and where γ, γ_2 are the activity coefficients of the fluid:

$$k_B T \ln(\gamma_i) = \frac{1}{N_0}\frac{\partial U_C}{\partial n_i}. \tag{9}$$

One can see that the interactions reduce the energy scale for the inclusion of monopoles at finite density: $|\tilde{\mu}| < |\mu|$ and $\gamma < 1$, leading to an increased monopole concentration compared to the noninteracting gas in the ratio $1/\gamma$ [45].

From this, all thermodynamic quantities for the monopole fluid can be calculated. For example, the magnetic specific heat transforms, in this representation to

$$C_{\mu,\mu_2} = \left(\frac{\partial}{\partial T}\right)(U_C - \mu N - \mu_2 N_2) = -N_0\left[\tilde{\mu}\left(\frac{\partial n}{\partial T}\right) + \tilde{\mu}_2\left(\frac{\partial n_2}{\partial T}\right)\right]. \tag{10}$$

Hence, if one can deal successfully with the Coulomb energy, one can give a complete self-contained description of the magnetolyte fluid in which the spin and magnetic charge degrees of freedom have been included independently, rather in the spirit of the gauge mean-field theories used to study quantum spin liquids [46].

The lowest order approximation is to neglect the Coulomb interaction altogether, giving a noninteracting lattice fluid apart from hard core repulsions. In this case $\tilde{\mu}$ and $\tilde{\mu}_2$ are equal to the respective chemical potentials and the problem is trivially solved. This is equivalent to a single tetrahedron approximation for the NNSI model [17] with $J_{\text{eff}} = -\mu/2$. The specific heat of the NNSI is accurately described by the single tetrahedron model (although not the susceptibility [47]) everywhere in the spin ice phase. For $\mu > 0$, the noninteracting monopoles crystallize via an order by disorder transition to the all-in-all-out phase [38], but this transition is not captured using the Pauling approximation for the entropy, Eq. (5). In the next section we go beyond the noninteracting case, adapting Debye-Hückel theory (see, e.g., Refs. [45,48]) to the magnetolyte.

B. Debye-Hückel theory

Debye-Hückel theory [1,17,48] uses the linearized Poisson-Boltzmann equation to go beyond mean-field theory, predicting a correlation induced electrostatic potential $\psi(r)$, a distance r from a test charge $q = zQ$, with z an arbitrary constant:

$$\psi(r \geqslant a) = z\left(\frac{\mu_0 Q}{4\pi r}\right)\frac{\exp[-(r-a)/\ell_D]}{1 + a/\ell_D}, \qquad \ell_D = \sqrt{\frac{k_B T}{Q^2 \rho_I \mu_0}}, \tag{11}$$

where ℓ_D is the Debye length. The short distance cutoff is, in our case, the lattice spacing a of the diamond lattice, $\rho = N/V$, $\rho_2 = N_2/V$ are the volume densities of charges, and $\rho_I = \rho + 4\rho_2$ is the interaction strength [48] for the magnetolyte with single and double charged monopoles. The test charge induces a charge cloud in its vicinity of opposite sign, whose extension is controlled by ℓ_D. The Coulomb energy is the energy required to place the test charge in the induced potential. It can be calculated using the Debye charging procedure in which the charge on each site is built up adiabatically for fixed particle correlations. Setting $Q(\lambda) = \lambda Q$, the Coulomb energy for the test charge at infinitesimally small λ is defined

$$\delta u(\lambda) = -z\lambda Q \psi(a, \lambda) = -z^2\left(\frac{\mu_0 Q^2}{4\pi a}\right)\frac{\lambda^2}{1 + (a\lambda/\ell_D)}. \tag{12}$$

This expression can now be integrated from $\lambda = 0$ to $\lambda = 1$ to find the Coulomb energy of the test particle $z^2 u^{\text{DH}}$. Taking the test charge to be a single ($z = 1$) or a double ($z = 2$) monopole gives the internal energy $U_C^{\text{DH}} = N_0 n_I u^{\text{DH}}$, with $n_I = n + 4n_2$ being the ionic strength:

$$U_C^{\text{DH}} = -\frac{N_0 k_B T}{6\pi\sqrt{3}}\left[\ln\left(1 + \frac{a}{\ell_D}\right) - \left(\frac{a}{\ell_D}\right) + \frac{1}{2}\left(\frac{a}{\ell_D}\right)^2\right]. \tag{13}$$

To convert the extensive variable from volume to N_0 we have used the volume per diamond lattice site $\tilde{v} = 8a^3/3\sqrt{3}$

[30]. Note that, as $\ell_D \propto 1/\sqrt{n}$, $U_C^{\rm DH} \sim n^{3/2}$ at low monopole density, contrary to the n^2 behavior typical of mean-field descriptions of short-range systems.

Minimizing Ω with respect to n and n_2 gives the effective chemical potentials

$$\tilde{\mu} = \mu + \Delta^{\rm DH}, \quad \tilde{\mu}_2 = \mu_2 + 4\Delta^{\rm DH},$$
$$\Delta^{\rm DH} = k_B T \frac{\ell_T}{\ell_D + a}, \tag{14}$$

and activity coefficients,

$$\gamma = \exp(-\beta\Delta^{\rm DH}), \quad \gamma_2 = \exp(-4\beta\Delta^{\rm DH}). \tag{15}$$

Here it is convenient to introduce the Bjerrum length $\ell_T = \frac{\mu_0 Q^2}{8\pi k_B T}$, at which the Coulomb interaction per monopole is equal to the thermal energy scale. The limiting law [1,33] for low ionic strength $(1-\gamma) \propto \text{const.}\sqrt{n_I}$, follows from Eq. (15).

Putting $\tilde{\mu}$ and $\tilde{\mu}_2$ into Eq. (7) and solving self-consistently for the densities [30] gives the Debye-Hückel equations of state $n(\mu, \mu_2, T)$ and $n_2(\mu, \mu_2, T)$ from which all thermodynamic quantities follow.

The details of the calculation can be considerably simplified by setting $\mu_2 = -\infty$ and restricting to the primitive (14-vertex) magnetolyte which can be compared in detail with the primitive electrolyte of Ref. [30]. This is justified for spin ice materials at low temperatures where the double monopoles can be neglected and is a practical simplification over the whole temperature range.

C. Limits of validity and charge pairing

Restricting to the primitive model for simplicity, the Poisson-Boltzmann equation for the induced potential $\psi(r)$ is

$$\nabla^2\psi(\vec{r}) = -\frac{\mu_0\rho Q}{2}\{\exp[-\beta Q\psi(\vec{r})] - \exp[\beta Q\psi(\vec{r})]\}, \tag{16}$$

where the equilibrium charge (volume) density for each species $\rho^{\pm} = \pm\frac{Q\rho}{2}$. This is solved in Debye-Hückel theory by keeping the linear terms in the exponential. This is a very poor approximation for $r < \ell_T$ so that the theory essentially ignores excess charge at distances less than this [49]. The validity of the Debye-Hückel U_C as the leading contribution to the Coulomb energy therefore depends on the contribution made by such near neighbors and the ratio of lengths $\frac{\ell_T}{\ell_D}$ is a good small parameter for this. At high temperature $\ell_T \to 0$ while ℓ_D diverges as $a\sqrt{\frac{k_B T}{u_a}}$. At low temperature one can use a pair approximation and treat near neighbor pairs as a species in chemical equilibrium. Their contribution to internal energy scales as n^2 at small density, compared to $n^{3/2}$ for the Debye-Hückel contribution [2,4,7,50].

As a consequence one expects the theory to be valid at both low and at high temperatures. The Debye-Hückel contribution to thermodynamic observables is measured by the activity coefficient, or $\Delta^{\rm DH}$, for which the low and high temperature limits are

$$\Delta^{\rm DH}(T \to 0) \sim u_a\sqrt{\frac{u_a n}{k_B T}}, \quad \Delta^{\rm DH}(T \to \infty) \sim u_a. \tag{17}$$

As the low temperature limiting law gives $\Delta^{\rm DH}$ varying as $\sqrt{n}$ only, one finds significant and experimentally observable contributions even for small charge concentrations [33]. At high temperature $\Delta^{\rm DH}$ is temperature independent, yet finite, illustrating the importance of screening even in this limit.

The short-range ionic pairing neglected by Debye-Hückel theory generates a contribution to the activity coefficient linear in ionic strength [50]. We develop pairing approximations for both the electrolyte and magnetolyte, whose details we give in Appendix D, and whose results appear in Figs. 1(e) and 1(f). For spin ice, our method enumerates the partition sum of two neighboring tetrahedra (corresponding to seven spins, i.e., $2^7 = 128$ vertex states), with the statistical weights adjusted by Bjerrum-like association constants.

This approach is specific to spin ice, because its short-range structure differs from that of a lattice electrolyte. The specificity of pairing contrasts with and underscores the universality of Debye-Hückel theory. Moreover, the improved match between theory and experiment (Fig. 1), achieved by adding the pairing correction, reveals that the small remaining discrepancy between DH theory and the experimental spin ice specific heat is also due to electrostatic correlations, with only a small part accounted for by the error of the Pauling approximation. This confirms spin ice as an experimental realization of a symmetric lattice electrolyte.

D. Comparison with electrochemical thermodynamics

To make contact with thermodynamics of an electrochemical process we take N, N_2 and the number of vacancies $N_v = N_0 - N - N_2$ as the extensive variables of a double chemical equilibrium such as that for water ice, Eq. (1). There is a quantitative equivalence here, with N_v corresponding to the number of neutral water molecules, N of the sum of the number of OH_3^+ and OH^- ions, and N_2 the sum of doubly charged ions, but this example can be taken as a test case within a more general framework.

The double equilibrium ensures that the three quantities are not independent. Their ratio is fixed by the equilibrium condition on the three chemical potentials, $2\mu_v = \mu_m + \mu_{2m}$. Thermodynamics further ensures that at least one independent variable imposed by the experimental setup is extensive. For spin ice, a suitable conserved quantity is clearly the number of tetrahedra N_0, corresponding in water ice to the number of oxygen ions. As a tetrahedron can be in one of several internal states, it is necessary to specify a thermodynamic reference state with a defined partition, with respect to which excess chemical potentials can be defined.

The choice is arbitrary. One could choose the cells to be all vacancies or create them by pairs and stipulate that they all be monopoles or double monopoles. However, our choice is clear—the excited state of the tetrahedron is selected following the vertex probabilities: $P_V = \frac{3}{8}$, $P_m = \frac{1}{2}$, and $P_{2m} = \frac{1}{8}$ which is the high temperature limit of the lattice gas. The chemical potential for the creation of such a tetrahedron is μ_0, so that $\mu_m = \mu_0 + \mu$ and $\mu_{2m} = \mu_0 + \mu_2$. Imposing N_0 rather than μ_0, the remaining thermodynamics modifies the internal partition, which is governed by the excess values μ and μ_2 only.

A suitable thermodynamic potential is then the Gibbs potential, parametrized to take into account the chemical equilibrium $G(T, P, N_0, \mu, \mu_2)$ and this is the usual starting point for treating water and ice. From this one can define the Helmholtz potential $F(T, V, N_0, \mu, \mu_2) - PV$. Putting volume $V = v_0 N_0$ and taking an incompressible approximation, V and N_0 will carry the same information, so that finally $F(T, V, N_0, \mu, \mu_2) \to \Omega(T, N_0, \mu, \mu_2) = U(S, N_0, N, N_2) - ST - \mu N - \mu_2 N_2$, which is our Eq. (3). Spin ice therefore provides a skeleton for the thermodynamics of electrochemical processes which includes numerous attractive simplifications compared to standard experimental systems. From this comparison with chemical thermodynamics it is clear that our approach should be considered as only semigrand canonical [51] with respect to the full set of thermodynamic variables, as only the internal degrees of freedom of the tetrahedra, or the chemical elements, are allowed to fluctuate.

Note that the reference state differs from the usual chemical choice, which is an ideal gas state. There are five different species, vacancies plus monopoles with ± 1 and ± 2 times the fundamental charge, so that in an ideal gas mixture the ratio of vacancies, monopoles, and double monopoles would be $\frac{1}{5}$, $\frac{2}{5}$, $\frac{2}{5}$. Hence, if μ_0 is an ideal gas chemical potential and relates to such a state, the number density of an ideal gas of monopoles would be $n = \frac{2}{5}\exp(\beta\mu)$, where μ is again an excess term. The lattice gas is far from an ideal gas, having particle exclusion over and above the Coulomb interactions. Hence, compared to an ideal gas there would be a nonzero activity coefficient even in the absence of Coulomb energy and for $\mu = 0$. For the lattice gas one can write $n = \frac{2}{5\gamma_{id}}\exp(\beta\mu)$ and setting $n = 1/2$ for $\mu = 0$ we get $\gamma_{id}^0 = \frac{4}{5}$. For general μ and μ_2, to equate the activity coefficients one has to solve the equation

$$\frac{2}{5\gamma_{id}} = \frac{\frac{4}{3\gamma}}{1 + \frac{1}{3}\left[\frac{4}{\gamma}\exp(\beta\mu) + \frac{1}{\gamma_2}\exp(\beta\mu_2)\right]}. \tag{18}$$

IV. TESTS OF THE THEORY

A. Magnetolyte simulations

In Fig. 2 we show specific heat data for systems with $\mu = -5.7$ K and $\zeta = 0.54$, as for HTO. We show simulation data for both the primitive electrolyte and magnetolyte (see Appendix C for methods). Notice that the areas under the curves are significantly different. This is a consequence of the constrained magnetolyte having a significantly different entropy change going from low to high temperature. The total entropy at high and low temperatures, which can be estimated from Eq. (5), are $S_\infty/N_0 k_B = \ln 7/2$ and $S_0/N_0 k_B = \ln 3/2$ for the magnetolyte and $S_\infty/N_0 k_B = \ln 3$ and $S_0/N_0 k_B = 0$ for the electrolyte, respectively. The inset shows the effect of including double monopoles to the magnetolyte. As can be seen, they modify the specific heat from 2 K and above.

To illustrate the expectations based on Debye-Hückel theory, we show in Fig. 3 simulation and theory for interaction parameters $\zeta = 0.27$, 0.54, and 0.71, the latter two corresponding to HTO and DTO and the first to a fictitious weakly interacting XTO, with half the pairwise Coulomb energy of HTO. Data are shown for a primitive magnetolyte and an

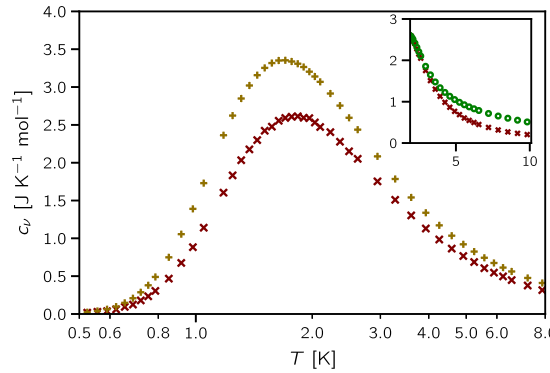

FIG. 2. Specific heat: Simulation data vs T for the primitive electrolyte (yellow crosses) and primitive magnetolyte (red crosses) for $\zeta = 0.54$, as for HTO. Inset: Primitive and full (16-vertex) magnetolyte (green circles) illustrating the effect of double monopoles on specific heat above 2 K.

electrolyte in each case and is plotted as a function of $\frac{k_B T}{\mu}$. In this form, the evolution in the data is uniquely due to the changing interaction strength. Also shown in each figure as a reference is the data for the noninteracting lattice gas.

From the XTO results one can see that Debye-Hückel theory does approach an exact description of the specific heat in the weakly interacting limit for the electrolyte. For the magnetolyte, although the theory is excellent, a small discrepancy between simulation and data can still be observed. This discrepancy between magnetolyte and electrolyte is because, in the former, charge pairs form a stronger correction (see Appendix D). A smaller part of the discrepancy is because we have the additional approximation of including the vacuum entropy within the Pauling approximation [30,52]. The error of Pauling approximation is due to correlations on the level of loops of six spins and longer. The loops also cause an error of similar order between our approximate entropy in Eq. (5) and the full entropy of spin ice with monopoles, and their contribution to spin ice entropy was estimated in Ref. [53].

As the interactions increase, the specific heat peak sharpens and moves to lower temperature. Deviations between Debye-Hückel theory and simulation develop as the theory correctly predicts the shift in peak position, but underestimates the sharpening. This sharpening is captured by our magnetolyte-specific pairing theory. However, for the interaction strengths of the real materials there remains excellent qualitative agreement which indeed becomes quantitative at both high and low temperature. In comparison, the noninteracting model appears in error at both high and low temperature and gives only a poor qualitative description of the Schottky peak. Closer examination at low temperature shows an asymptotic approach towards the simulation results below 0.5 K, as the monopole density falls to zero [17]. At high temperature the data always disagree, illustrating the importance of screening in a Coulombic system even in this limit.

B. Experiment

The heat capacities of the spin ices $Dy_2Ti_2O_7$ and $Ho_2Ti_2O_7$ were measured between 0.35 and 300 K by a heat-relaxation method, using a Quantum Design Physical Properties Measurement System (PPMS), equipped with a

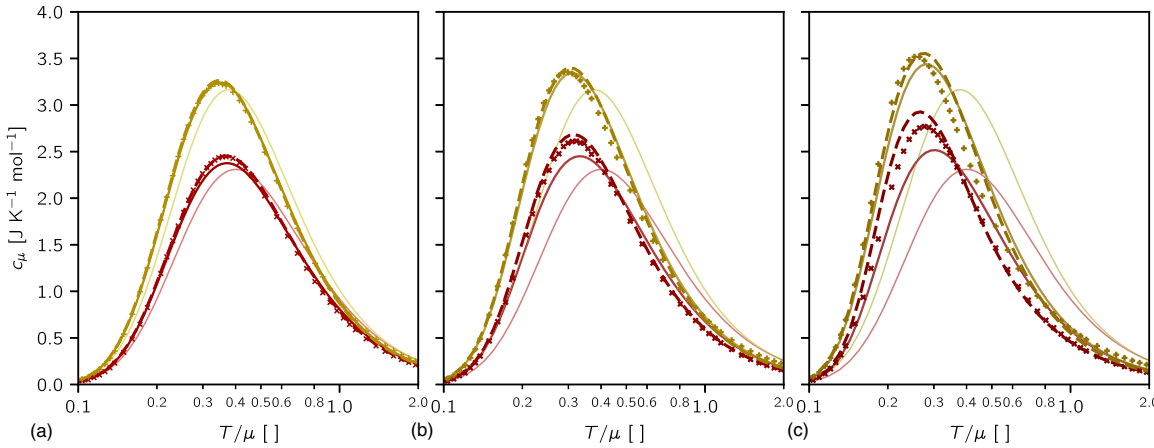

FIG. 3. Specific heat: Simulation data vs T/μ for the electrolyte (yellow crosses) and primitive magnetolyte (red crosses) with corresponding Debye-Hückel theory (yellow full line and red full line) and its pairing extension (yellow dashed line and red dashed line). The pairing correction is negligible for the weakly coupled system (left panel) but its significance increases as the Coulomb interaction strengthens. The exact specific heat for noninteracting particles is shown for reference (light yellow and light red lines. (a) With $\zeta = 0.27$ (see text), (b) with $\zeta = 0.54$, as for HTO, and (c) $\zeta = 0.71$ as for DTO.

^{3}He option. An addendum measurement was made to evaluate the background of Apiezon Grease N and this contribution was subtracted from the data. Three repetitions were taken for each measurement to improve statistics.

The equilibrium heat capacity may be modeled as the sum of nuclear (hyperfine), electronic, and lattice heat capacities. The electronic contribution, which interests us here, may be isolated by correcting the total specific heat for the nuclear and lattice specific heats. For $Ho_2Ti_2O_7$ the hyperfine parameter $A = 0.30$ K is accurately known [54], but the correction for the nuclear specific heat becomes very large at low temperature; we estimate that systematic errors arising from the subtraction of this contribution to be negligible above $T \approx 0.8$ K and very small (a few percent) down to 0.4 K. For $Dy_2Ti_2O_7$ the nuclear contribution is smaller, but the nuclear spin relaxation rate is quite slow and comparable to experimental timescales at low temperature. In other work [55] we derived a robust estimate of the electronic contribution by comparing short time and long time measurements with measurements on an isotopically enriched sample with no nuclear contribution. We have also estimated bounds on the variation of specific heat caused by slow equilibration of the electronic spin system. In this way we estimate that systematic errors arising from such sources are entirely negligible above $T \approx 0.8$ K and very small (again no more than a few percent) down to 0.4 K. As regards the lattice (phonon) contribution we found that a T^3-type correction is inadequate for an accurate measurement of the electronic specific heat. Note that such a correction has been used in the past for spin ice materials [56,57]; but if the object is estimating entropy, as has usually been the case, then the error incurred is small. By detailed comparison with the case of $Tb_2Ti_2O_7$ [58], we have established the accuracy of a correction for the lattice contribution that involves comparing with the measured heat capacities of nonmagnetic $Y_2Ti_2O_7$ and $Lu_2Ti_2O_7$. These are isostructural to the spin ices but have different Debye constants. A simple temperature scaling gives a collapse of the phonon heat capacities over an acceptable range of temperature. Analysis of the corrections showed that systematic errors in the estimated electronic specific heat of the spin ices become negligible at temperatures less than $T \approx 8$ K.

Summarizing these factors, in Fig. 1, we display the estimated electronic specific heat in the range 0.4–10 K, but emphasize that systematic errors can only be completely excluded in the more restricted range 0.8–8 K, as discussed above. It is evident from the figures that the theory with monopole pairing included is very satisfactory in both cases. In general the description is slightly more accurate for $Ho_2Ti_2O_7$ than for $Dy_2Ti_2O_7$ as would be expected from the fact that $Ho_2Ti_2O_7$, having the larger $|\mu|$, and hence a lower charge density, corresponds more accurately to the Debye-Hückel linear approximation. Further discussion of systematic errors in the comparison of theory and experiment is given in Appendix A.

V. CONCLUSIONS

We first consider our results in the magnetic context and subsequently consider their implications for the electrochemistry. In magnetic terms, our analysis of the magnetolyte provides a theoretical description of specific heat of the complex frustrated magnetic system spin ice, to an unprecedented level of accuracy. We have demonstrated that the monopole picture provides a framework for thermodynamics of spin ice going beyond existing techniques such as mean-field theory, single tetrahedron, or Bethe lattice calculations [47]. Using Debye-Hückel theory and its extensions we find a quantitative description of spin ice over a full range of temperatures, whereas the previous work has only approximately dealt with low temperatures [30]. This kind of development has so far proved beyond the capacity of the spin picture, illustrating that the magnetolyte takes us a step beyond the dipolar spin ice model from which it is derived.

Our description of the magnetolyte affords an efficient approach to charge correlations that emphasizes the role of the strongly correlated monopole vacuum in spin ice. The price one pays for this step however, is to neglect the finite energy scale of the bandwidth of Pauling states. This has important

consequences, particularly at low temperature where ordering [41] and corrections to spin ice physics [44,55] cannot straightforwardly be accounted for. We note that it is, at any rate, very remarkable that it is possible to describe a spin system in terms of its emergent *low-energy* fractionalized degrees of freedom across the *full* temperature range. We are not aware of another instance that is not otherwise exactly soluble anyway, where this is possible.

The Debye-Hückel approach presented here can be used to calculate other properties of spin ice. For example solution of the linearized Eq. (16) gives the Green's function for a key equation discussed in Ref. [59] [coincidentally labeled there Eq. (16)]. That equation was shown to capture, over the entire temperature range, the "pinch point" [60] and "harmonic phase" [59] spin correlations in spin ice, as observed by polarized neutron scattering [61]. Indeed we anticipate that our analysis, with its pairing corrections, should accurately describe all the magnetic thermodynamics of the classic spin ice materials, from specific heat to wave-vector-dependent susceptibility. It further gives a starting point to calculate corrections to the Arrhenius law relaxation [30,62,63] observed experimentally (some of which show Vogel-Fulcher behavior [63]) and in the future could be used to analyze the properties of epitaxial spin ice interfaces that are now within experimental reach [64,65].

Our main conclusion, however, goes way beyond the physics of spin systems and relates to the broader context of electrochemistry. We have shown here that spin ice models and materials provide a model testing ground for Coulombic lattice fluids in which the separation of energy scales allows us to isolate the essential degrees of freedom for Coulomb driven phenomena. In this regard, the magnetolyte is unique in several aspects: exact charge symmetry, absence of solvent, and precise control of the chemical potential. This charge symmetry makes spin ice an essentially perfect realization of the restricted primitive model, which allows for many simplifications to analytical calculations. As a consequence the complex frustrated magnet has becomes an experimentally accessible model system for theories addressing the correlations of Coulomb fluids [15].

We have shown that the grand canonical lattice Coulomb fluid corresponds, in a wider thermodynamic setting to a semigrand canonical formulation in which only excess chemical potentials play a role and that this is a natural starting point for many electrolyte systems. Spin ice therefore presents a simple framework for electrochemical thermodynamics and offers many technical and practical reasons for choosing spin ice to address modern problems. The excess chemical potentials of the magnetolyte can be determined accurately and are fixed parameters, independent of temperature. This is, because the monopoles have no kinetic energy unlike dissolved ions, as all kinetic energy is electronic, quantized, and fully contained in the magnetic terms of the Hamiltonian. As a consequence, there is a broad choice of the value of the chemical potential, as well as the Coulomb coupling, which can be further tuned by chemical pressure [66], while staying remarkably stable under hydrostatic pressure. This does away with the need to consider the evolution of the thermal de Broglie wavelength and the kinetic energy with temperature, unlike in the lattice electrolytes of Ref. [8], thus further anchoring the chemical potential. It is this that allows us to treat the system as a stochastic lattice gas and to choose a reference state with respect to it. Unlike standard chemical approaches [67] we do not use an ideal gas state as the reference state. This is, in part because of the absence of kinetic energy and in part due to the underlying translational symmetry of the lattice which invites the use of a lattice fluid formalism and which considerably simplifies the calculations.

The absence of solvent allows us to model electrostatic correlations exclusively without having to consider solvation effects, such as the temperature dependence of interactions due to varying dielectric constant. Neither is there an effect of electrostatic interactions on the chemical potential of the solvent, because the number of ground state (empty) sites of the magnetolyte is fixed by the number of charges. This means that the osmotic coefficient [10] is always unity. Finally, the absence of solvent allows for the 20-fold variation in temperature in our experiments, which is larger than the ratio between evaporation and freezing temperatures of most common solvents.

Improved experimental technique and data analysis are indispensable for the precise match between theory and the experimental specific heat data. As spin ice physics takes place in the 1 K temperature range, the magnetic degrees of freedom separate easily from lattice vibrations, allowing for measurements over a particularly wide range of temperatures. For example, the data in Figs. 1 and 3 is over a range $0.1 \lesssim \frac{k_B T}{\mu} \lesssim 2$, covering both the high and low temperature regimes. To obtain this range we have presented new experimental data for specific heat of $Ho_2Ti_2O_7$ and $Dy_2Ti_2O_7$ with an improved analysis regarding the subtraction of nonmagnetic effects.

Following this success, future experiments should push outside this comfort zone into regions where Debye-Hückel-Bjerrum theory breaks down providing an environment where new theoretical ideas can be tested. Reducing the scale of the chemical potential would take spin ice materials beyond $Dy_2Ti_2O_7$, into the strongly interacting region and towards the crystallization transition where this is the case. This can be achieved by changing the ratio of exchange to dipolar interaction by applying physical pressure, or by replacing the nonmagnetic ion with species of a different radius. For example, replacing Ti^{4+} by the smaller Ge^{4+} considerably reduces the scale of μ [31] and this could be further changed by performing experiments under pressure. It would be interesting in future experiments to revisit $Dy_2Ge_2O_7$ in this context.

One such area is that of confined Coulomb fluids at high charge density, for which Debye-Hückel theory and extensions fail spectacularly, where the respective authors of Refs. [14,15] speculate that screening is mediated by "Schottky defects" in place of ions. Numerical and experimental work in confined primitive systems is potentially extremely useful here for the development of a phenomenological picture of the processes involved. In particular we note that spin ice can be *continuously* tuned from a monopole conductor to a Schottky defect conductor, as shown previously in Ref. [27].

Recent progress in spin ice experiment and theory has also targeted thin film development [64,65,68]. Thin spin ice films could bring a testing ground for anomalous phenomena observed and predicted within confined electrolytes and ionic liquids [69–72]. While bringing together these two fields at

a quantitative level is certainly challenging, the rewards at both the fundamental and the technological level are high. As a noteworthy analogy, we can mention water-air interface, which is acidic, i.e., attracts excess protons [73]. Spin ice surface too possesses fluctuating excess monopoles on its surface due to "open" Dirac strings. However, unlike in the case of water-air interface, this charge is tuneable by field or doping [74].

Finally, our "autoionization" scheme, Eq. (1), means that our results are relevant to pure liquid water. They appear to clear up one seemingly overlooked issue in the electrochemistry of this most important of electrochemical systems. In particular, among several promising approaches to water [75], one puts particular emphasis on ice-rule correlations [76]. This makes water, like its solid form ice [77], a highly correlated system and raises the question, how can such a highly correlated system be treated with standard chemical thermodynamics that assumes the statistical independence of chemical species? The answer is contained in our analysis that shows how the assumption of statistical independence is justified by the Pauling approximation, which restores the independence of the (effective) chemical species in Eq. (1), and allows standard methods to be applied over a range of temperatures. Hence our result supports the contention that chemical thermodynamics applies to liquid water, even though it is far from being a passive solvent for hydrogen ions [75]. It is interesting to note that the autoionization of water remains a subject of intense debate in the literature [78,79].

To conclude, spin ice is a rare example of an experimentally accessible grand-canonical Coulomb fluid with varying interaction strengths in which one can confront Debye-Hückel theory and test systematic improvements to it. Furthermore, other electrolyte effects, such as their nonlinear response, can be observed in spin ice, as authors of this paper have previously shown theoretically [80] and experimentally [81]. In the future, phenomena that could be probed in this model material include confinement of electrolytes [64,65] and the role of quenched disorder and glassiness in long-range interacting systems [82].

ACKNOWLEDGMENTS

It is a pleasure to thank L. D. C. Jaubert, M. J. P. Gingras, A. Sen, C. Castelnovo, and S. Sondhi for many fruitful discussions about spin ice and its models, as well as for collaboration on related work. This work was in part supported by the Deutsche Forschungsgemeinschaft via Grant SFB 1143. L.B. was supported by the Leverhulme Trust through the Early Career Fellowship program (ECF2014-284).

APPENDIX A: FURTHER DISCUSSION OF SYSTEMATIC ERRORS IN THE COMPARISON OF THEORY WITH EXPERIMENT

In addition to the sources of systematic error described in the main text (i.e., inaccuracies in the Debye-Hückel linear approximation, and in the experimental correction for the nuclear and phonon contributions to the specific heat) there are several more subtle sources of systematic error that appear in our comparison of theory and experiment.

The dipolar spin ice parameters describing $Dy_2Ti_2O_7$ and $Ho_2Ti_2O_7$ were originally estimated by fitting experimental data for specific heat divided by temperature c/T to numerical simulations of the dipolar spin ice model (DSI) [26]. These parameters were later used to infer the parameters of the magnetolyte model [22]. We have finally used these magnetolyte parameters to calculate the specific heat within extended Debye-Hückel theory, which is then compared with experiment.

Like the DSI, the magnetolyte model has three parameters: $\{Q, a, \mu\}$ where DSI has $\{g, a, J\}$. Here Q is the monopole charge, a is the cubic lattice parameter, μ is the monopole chemical potential, g is the rare earth g factor, and J is an exchange coupling. Small systematic differences between theory and experiment appear in approximating the real materials to DSI, in the original choices of g and a, and in approximating the DSI to the magnetolyte model. Of these only the values of g and a can be freed from systematic errors by more accurate measurements, but this is barely worthwhile given the fundamental systematic differences between DSI, the magnetolyte model, and the experimental systems. These factors contribute systematic errors of order 1% in the comparison of theory and experiment for the specific heat.

The magnetolyte reproduces the specific heat of both experiment and the DSI to high accuracy above around 0.4 K. Below this temperature the models differ as the DSI orders [83] due to the finite bandwidth of Pauling states. Spin correlations are modified by this energy scale and extra parameters are required in the DSI to describe neutron scattering at low temperature (for example) [84]. The physics related to this energy scale is completely neglected in the magnetolyte but our results show that it does not affect the monopole thermodynamics over the temperature range 0.4–10 K.

APPENDIX B: DISCRIMINATING BETWEEN DOUBLE DEFECTS IN ELECTROLYTES AND MAGNETOLYTES

In Fig. 4 we show simulation data for the full magnetolyte, together with the corresponding Debye-Hückel theory. Also shown are alternative theoretical approaches that capture the different many-body effects at play: noninteracting theory, Debye-Hückel theory for the primitive magnetolyte, and for an electrolyte including double charges. All fail to capture the simulation data as discussed in the main text. Including double charges for the electrolyte produces a clear second feature at higher temperature, corresponding to the thermal excitation of the second species. Although the effect of double monopoles is clearly observable in the simulation, such a pronounced double feature is not present in the magnetolyte as their weight is constrained by the vertex counting [see Eq. (5) and discussion].

APPENDIX C: MONTE CARLO SIMULATIONS

To obtain the simulation data in this article, we performed Monte Carlo simulations of the dumbbell model of spin ice. We used four types of Monte Carlo steps: single spin flips (`S`), monopole moves (`M`), charged worms (`C`), and loop flips (`L`). Single spin flips attempt to flip a random spin in the system ($2N_0$ times per step), which moves a charge or

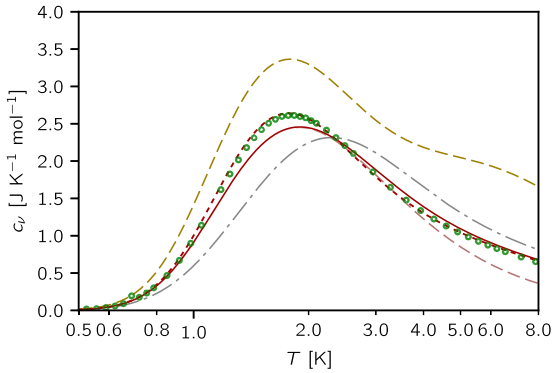

FIG. 4. Comparing simulation specific heat of double defect dumbbell model (green circles) with a variety of theories illustrates different contributions to the specific heat: simulation data for $\zeta = 0.54$ as for HTO, including double monopoles. Theoretical curves: Noninteracting magnetolyte (gray dashed), Debye–Hückel theory with single monopoles only (red dashed), Debye-Hückel theory for the electrolyte including double charges (yellow dashed), Debye-Hückel theory for magnetolyte including double charges (solid brown), and with pairing considered (dotted brown).

creates/destroys a nearest-neighbor $(+-)$ charge pair. We also keep a list of monopoles that we randomly choose from to propose a move to one of the neighboring sites (N_0 times per step). Finally, the worm steps construct either a string of spins that flips while moving a charge across the system or a loop of spins that flips without changing. For our simulations we used the order `SMSLMSMLSMSC` of MC steps for each sweep. We used Metropolis update scheme for all MC steps.

TABLE I. Parameters of our MC simulations for $Dy_2Ti_2O_7$: temperature range, temperature step, system size, and the total number of sweeps.

T	ΔT	L	MC sweeps
2.25–10	0.25	6	100 000
1.6–2.0	0.1	8	100 000
0.90–1.55	0.05	8	100 000
0.60–0.85	0.05	10	100 000
0.55–0.575	0.025	12	100 000
0.50–0.525	0.025	16	100 000
0.475	0.025	20	100 000
0.450	0.025	24	10 000
0.425	0.025	32	10 000
0.400	0.025	40	10 000

The Coulomb energy was evaluated by Ewald summation with metallic boundary conditions at infinity. The specific heat was calculated using the fluctuation-dissipation theorem. All the above-mentioned methods are further detailed in Refs. [17,85].

The simulated system contains L^3 pyrochlore lattice unit cells, i.e., $8L^3$ charge sites and $16L^3$ spins. We adapted system size L to be larger than twice the Debye screening length (see Table I). The system size increases fast with the lowering temperature as the monopole number density increases exponentially. As the memory cost of the simulation increases, we reduce the total number of steps taken. Nevertheless, the worm algorithm ensures that the configuration space is sampled efficiently independent of the temperature and monopole density.

APPENDIX D: PAIRING THEORY

This Appendix serves to describe methods on how to include pairing as a next order correction in electrolytes and magnetolytes. We show that unlike the Debye-Hückel theory, the pairing theory is not transferable between electrolytes and magnetolytes due to their different short-range structure.

1. Electrolytes

Pairing in lattice electrolytes has previously been described in Ref. [8], which used the Bethe approximation for the monomer-dimer model as given by Nagle [86]. We adapt this approximation to include orientable dimers, i.e., dipoles, with results shown in Fig. 5. The number of configurations available for positive and negative charges, and for their oriented nearest-neighbor dipoles on a lattice:

$$W = \left[\binom{N}{\frac{Nn}{2}\ \frac{Nn}{2}\ Nn_b\ N(1-n-n_b)}(2q)^{Nn_b}\right]\left[\frac{n_b}{2q}\left(1-\frac{n_b}{q}\right)^{q-1}\right]^{\frac{Nn_b}{2}}\left[\left(1-\frac{n_b}{q}\right)^{q}\right]^{\frac{N(1-n_b)}{2}}, \tag{D1}$$

where the first bracket describes the possible placings of positive charges, negative charges, and their bound states (with number density n_b); $q = 4$ is the connectivity of the lattice; the latter brackets describe the compatibility of dimers and monomers with their neighboring sites.

The corresponding entropy reads

$$\frac{S}{Nk_B} = \frac{1}{N}\log(W) = -n\log\frac{n}{2} - (1-n-n_2-n_b)\log(1-n-n_b) - \frac{n_b}{2}\log\frac{n_b}{8} + \left(2-\frac{n_b}{2}\right)\log\left(1-\frac{n_b}{4}\right) \tag{D2}$$

and free energy

$$\frac{F}{N} = \frac{U}{N} - \sum_i n_i\mu_i - \frac{TS}{N} = -n\tilde{\mu} - \frac{n_b}{2}(2\mu + kT\log K_E)$$
$$- k_BT\left[-n\log\frac{n}{2} - (1-n-n_2-n_b)\log(1-n-n_b) - \frac{n_b}{2}\log\frac{n_b}{8} + \left(2-\frac{n_b}{2}\right)\log\left(1-\frac{n_b}{4}\right)\right], \tag{D3}$$

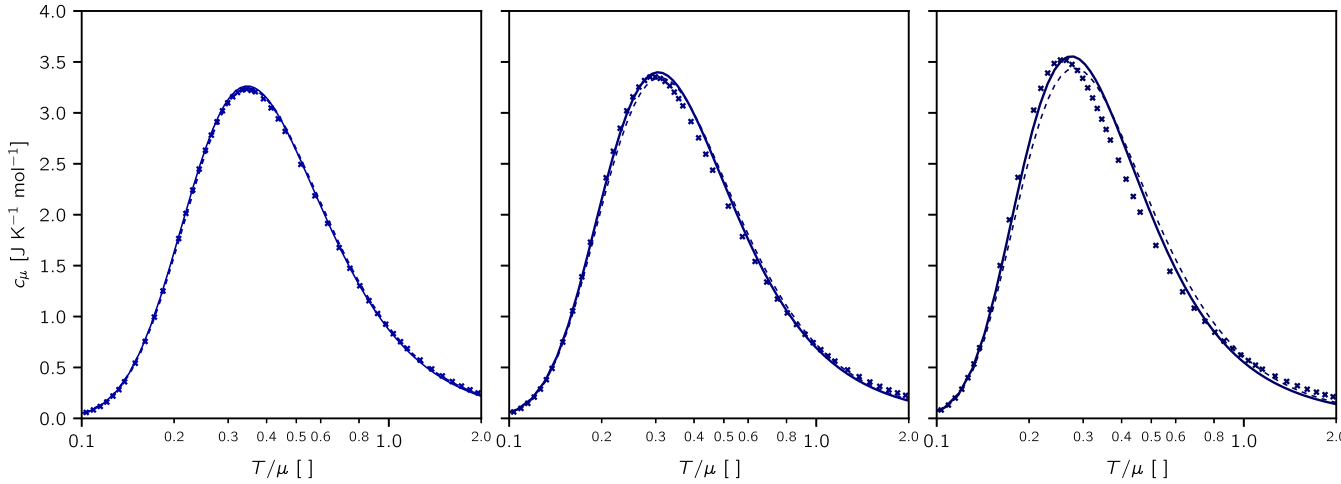

FIG. 5. Pairing theory for lattice electrolytes. Specific heat curves for electrolytes with μ and ζ of XTO, HTO, and DTO. Points are simulation results, dashed line the DH theory, full line the pairing theory. Temperature is given in units of the chemical potential.

where the chemical potential of the pairs follows from their chemical equilibrium with the free charges set by the truncated Ebeling association constant $K_E = \exp(-\beta U) + \exp(\beta U) - 2 - \frac{(\beta U)^2}{2}$. The continuous Ebeling constant is the integral of the previous expression over the whole space, which exactly captures the excess correlations in electrolytes to order l_D^2, while preserving the previously derived DH theory [50]. While it formally treats only the $+-$ association, Ebeling's theory in fact includes all correlations of this order, even between like charges. Due to the effort needed to calculate entropy of pairs of all sizes allowed by the diamond lattice, we only consider nearest neighbor pairs and truncate K_E.

The free energy can be minimized with respect to the number densities, yielding

$$n = \frac{6e^{\beta\tilde{\mu}}}{1 + 2e^{\beta\tilde{\mu}} + 2\sqrt{(1 + 2e^{\beta\tilde{\mu}})^2 + 6K_E e^{2\beta\mu}}}, \tag{D4}$$

$$n_b = \frac{(1 + 2e^{\beta\tilde{\mu}})^2 + 4K_E e^{2\beta\mu} - (1 + 2e^{\beta\tilde{\mu}})\sqrt{(1 + 2e^{\beta\tilde{\mu}})^2 + 6K_E e^{2\beta\mu}}}{\frac{1}{2}(1 + 2e^{\beta\tilde{\mu}})^2 + 4K_E e^{2\beta\mu}}, \tag{D5}$$

which limit to the DH theory for $K_E \to 0$. This approach can be easily extended to include double charges. The specific heat is obtained from Eq. (10) as in the main text.

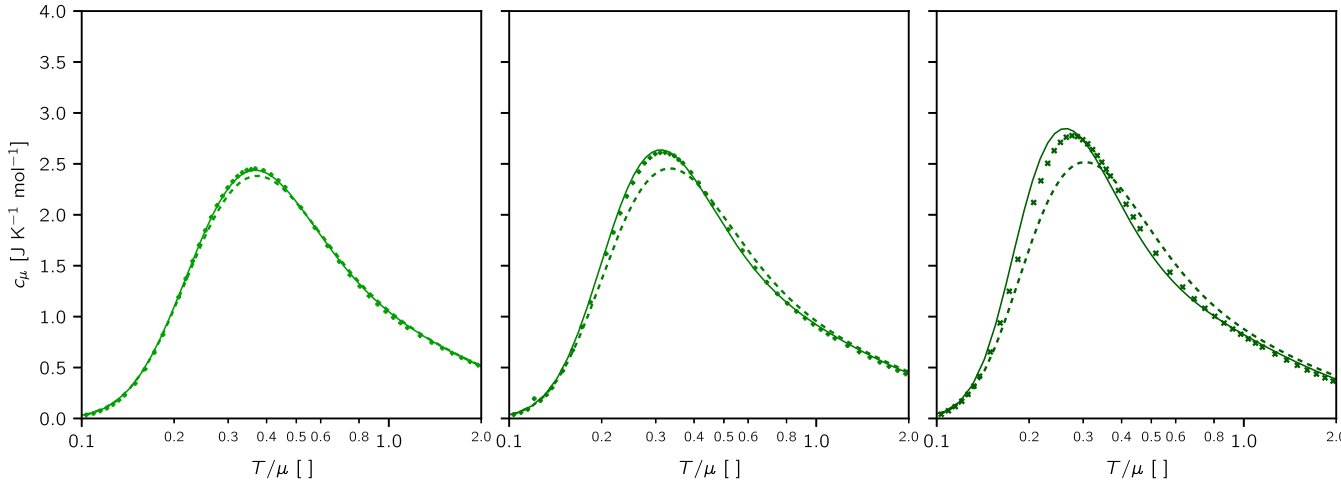

FIG. 6. Pairing theory for the double-defect magnetolyte. Specific heat curves for μ and ζ corresponding to XTO, HTO, and DTO. Points are simulation results, dashed line the DH theory, full line the pairing theory. Temperature is given in units of the chemical potential.

2. Magnetolytes

For spin ice, a different approach has to be taken, because every charge state is underpinned by multiple spin configurations. Nagle's argument about monomer-dimer compatibility fails completely because the compatibility of every vertex with its neighbor is fully determined by the orientation of the spin connecting them, which is always compatible with half of the vertex states. This makes compatibility of pairs with neighboring charges easier to achieve which, in turn, promotes pairing in comparison with electrolytes, as visible in Fig. 6. As an alternative, the calculation can be performed within the scope of a two-site (seven spins, with $2^7 = 128$ configurations) approximation. Six of the spins are shared with neighboring tetrahedra, while one spin is internal. The following number of spin configurations corresponds to given charge configurations:

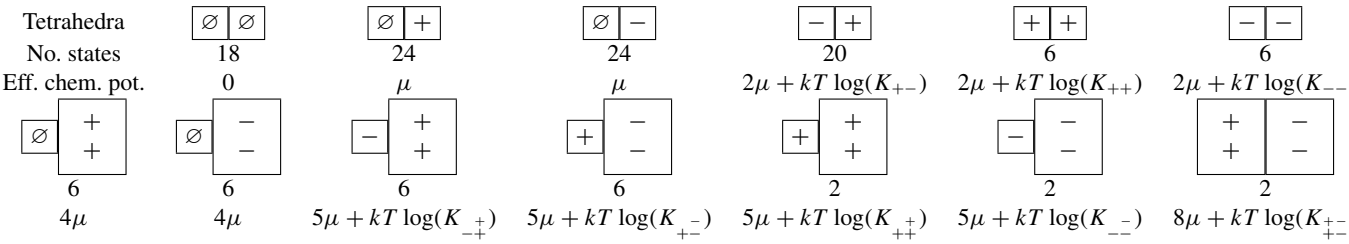

The electrostatic interactions can once again be included by replacing the chemical potential μ with the effective chemical potential $\tilde{\mu}$ from the DH theory. This constrains the association constants to limit to unity ($K \to 1$) in order to recover DH theory in the single-vertex nonpairing case, which excludes the Ebeling approach from above, and therefore we adopt Bjerrum-like association constants below. Other constraints on the association constants are the charge symmetry $K_{--} = K_{++}$ and the quadratic scaling with ionic strength $K_{+-} = K^2_{\ +-} = K^4_{+-}$.

The total number of configurations reads

$$W = \left(\frac{1}{2}\right)^{3N_0} \frac{N_0!}{N_1!N_2!\cdots N_{128}!}, \tag{D6}$$

where the 128 vertices are assigned the following charge identities $N_1 = N_2 = \cdots N_{18} = N_{\varnothing\varnothing}/18$, $N_{19} = \cdots N_{42} = N_{\varnothing+}/24$, $N_{43} = \cdots N_{66} = N_{\varnothing-}/24$, $N_{67} = \cdots N_{86} = N_{+-}/20$, $N_{87} = \cdots N_{92} = N_{++}/6$, $N_{93} = \cdots N_{98} = N_{--}/6$, $N_{99} = \cdots N_{104} = N_{\varnothing\ +}^{\ +}/6$, $N_{105} = \cdots N_{110} = N_{\varnothing\ -}^{\ -}/6$, $N_{111} = \cdots N_{116} = N_{-\ +}^{\ +}/6$, $N_{117} = \cdots N_{122} = N_{+\ -}^{\ -}/6$, $N_{123} = N_{124} = N_{+\ +}^{\ +}/2$, $N_{125} = N_{126} = N_{-\ -}^{\ -}/2$, $N_{127} = N_{128} = N_{-\ +}^{\ -}/2$, where the first and the second indices describe the charge at the respective diamond lattice sites.

This leads to the entropy per tetrahedron

$$\begin{aligned}\frac{S}{(N/2)k_B} = \frac{1}{N/2}\log(W) = &-n_{\varnothing\varnothing}\log\left(\frac{8n_{\varnothing\varnothing}}{18}\right) - n_{\varnothing+}\log\left(\frac{8n_{\varnothing+}}{24}\right) - n_{\varnothing-}\log\left(\frac{8n_{\varnothing-}}{24}\right)\\ &- n_{+-}\log\left(\frac{8n_{+-}}{20}\right) - n_{\varnothing\ +}^{\ +}\log\left(\frac{8n_{\varnothing\ +}^{\ +}}{6}\right) - n_{\varnothing\ -}^{\ -}\log\left(\frac{8n_{\varnothing\ -}^{\ -}}{6}\right)\\ &- n_{++}\log\left(\frac{8n_{++}}{6}\right) - n_{--}\log\left(\frac{8n_{--}}{6}\right) - n_{-\ +}^{\ +}\log\left(\frac{8n_{-\ +}^{\ +}}{6}\right)\\ &- n_{+\ -}^{\ -}\log\left(\frac{8n_{+\ -}^{\ -}}{6}\right) - n_{+\ +}^{\ +}\log\left(\frac{8n_{+\ +}^{\ +}}{2}\right) - n_{-\ -}^{\ -}\log\left(\frac{8n_{-\ -}^{\ -}}{2}\right) - n_{+-}^{+-}\log\left(\frac{8n_{+-}^{+-}}{2}\right).\end{aligned} \tag{D7}$$

If the chemical potentials for pairs of tetrahedra were simply sums of their components' chemical potentials, the free energy would factorize to the previously used single-vertex form. This factorization follows from the fact that we have not introduced any additional correlations (as we do not include any loop which would have a minimal size of six tetrahedra). This imposes the following relations on the single vertex densities:

$$\begin{aligned}&n_{\varnothing\varnothing} = n_{\varnothing}^2, \quad n_{\varnothing+} = n_{\varnothing-} = 2n_{\varnothing}n_+, \quad n_{+-} = \frac{5}{2}n_+n_-, \quad n_{++} = n_{--} = \frac{3}{4}n_+^2,\\ &n_{\varnothing\ +}^{\ +} = n_{\varnothing\ -}^{\ -} = 2n_{\varnothing}n_+^+, \quad n_{+\ -}^{\ -} = n_{-\ +}^{\ +} = 3n_+n_-, \quad n_{+\ +}^{\ +} = n_{-\ -}^{\ -} = n_+n_+^+, \quad n_{+-}^{+-} = 4n_+^+n_-^-,\end{aligned} \tag{D8}$$

and the symmetric relations are due to the macroscopic electroneutrality $n_+ = n_-$, $n_+^+ = n_-^-$.

We are now faced with the choice of the association constant. The simplest choice is to use the Boltzmann weight of the nearest neighbor charge pair $K_{+-} = \exp(-\beta U_{NN}) = \exp(2\ell_T/a) \overset{\text{def.}}{=} K$, $K_{++} = K_{--} = \exp(\beta U_{NN}) = \exp(-2\ell_T/a) = 1/K$,

$K_{-+}^{+} = K_{+-}^{-} = K^2$, $K_{++}^{+} = K_{--}^{-} = 1/K^2$, $K_{+-}^{+-} = K^4$. We also assume that all charges keep their DH correction to the chemical potential, yielding the free energy

$$\begin{aligned}\frac{F}{N/2} &= \frac{U}{N/2} - \sum_i n_i\mu_i - \frac{TS}{N/2}\\ &= -\mu n_{\varnothing+} - (2\mu + kT\log K)n_{+-} - (2\mu - kT\log K)n_{++}\\ &\quad - 4\mu n_{\varnothing+}^{+} - (5\mu + 2kT\log K)n_{-+}^{+} - (5\mu - 2kT\log K)n_{++}^{+} - (8\mu + 4kT\log K)n_{+-}^{+-}\\ &\quad - k_BT\left[n_{\varnothing\varnothing}\log\left(\frac{8n_{\varnothing\varnothing}}{18}\right) + 2n_{\varnothing+}\log\left(\frac{8n_{\varnothing+}}{24}\right) + n_{+-}\log\left(\frac{8n_{+-}}{20}\right) + 2n_{++}\log\left(\frac{8n_{++}}{6}\right)\right.\\ &\quad \left. + 2n_{\varnothing+}^{+}\log\left(\frac{8n_{\varnothing+}^{+}}{6}\right) + 2n_{-+}^{+}\log\left(\frac{8n_{-+}^{+}}{6}\right) + 2n_{++}^{+}\log\left(\frac{8n_{++}^{+}}{2}\right) + n_{+-}^{+-}\log\left(\frac{8n_{+-}^{+-}}{2}\right)\right].\end{aligned} \tag{D9}$$

This free energy can be truncated accordingly to include only singly charged configurations.

We minimize again with respect to the densities

$$\begin{aligned}&n_{\varnothing\varnothing} = 9/Z, \quad n_{\varnothing+} = n_{\varnothing-} = 12e^{\beta\tilde{\mu}}/Z, \quad n_{+-} = 10Ke^{2\beta\tilde{\mu}}/Z, \quad n_{++} = n_{--} = 3K^{-1}e^{2\beta\tilde{\mu}}/Z,\\ &n_{\varnothing+}^{+} = n_{\varnothing-}^{-} = 3e^{4\beta\tilde{\mu}}/Z, \quad n_{-+}^{+} = n_{+-}^{-} = 3K^2e^{5\beta\tilde{\mu}}/Z, \quad n_{++}^{+} = n_{--}^{-} = K^{-2}e^{5\beta\tilde{\mu}}/Z, \quad n_{+-}^{+-} = K^4e^{8\tilde{\beta}\mu}/Z,\end{aligned} \tag{D10}$$

where

$$Z = 9 + 24e^{\beta\tilde{\mu}} + 10Ke^{2\beta\tilde{\mu}} + 6K^{-1}e^{2\beta\tilde{\mu}} + 6e^{4\beta\tilde{\mu}} + 6K^2e^{5\beta\tilde{\mu}} + 2K^{-2}e^{5\beta\tilde{\mu}} + K^4e^{8\beta\tilde{\mu}}, \tag{D11}$$

which translates to free charge densities

$$n_\varnothing = \sqrt{n_{\varnothing\varnothing}} = \frac{3}{\sqrt{Z}}, \quad n = 2\frac{n_{\varnothing+}}{2n_\varnothing} = \frac{4e^{\beta\tilde{\mu}}}{\sqrt{Z}}, \quad n_2 = 2\frac{n_{\varnothing+}^{+}}{2n_\varnothing} = \frac{e^{4\beta\tilde{\mu}}}{\sqrt{Z}}. \tag{D12}$$

The specific heat is again obtained using the procedure outlined in Eq. (10) of the main text.

The limitation of this approach is that the we assume that even charges in dipoles keep the DH form of screening, which partially double counts the electrostatic interactions. A fully consistent approach would require a study of mean-field screening of all the nearest-neighbor charge configurations appearing in our expansion, as outlined for electrolytes in Ref. [6].

For both electrolytes and magnetolytes, pairing improves on the specific heat description using DH theory. However, the description of pairing in the two scenarios differs significantly, which demonstrates that short-range structure and the emergent nature of spin ice differs from lattice electrolytes, while long-range properties of spin ice and electrolytes match well.

[1] P. Debye and E. Hückel, Phys. Z. **24**, 185 (1923).
[2] N. J. Bjerrum, Det Kgl. Danske Videnskabernes Selskab., Math.-fysiske Meddelelser. **7**, 1 (1926).
[3] J. E. Mayer, J. Chem. Phys. **18**, 1426 (1950).
[4] M. Justice and J. Justice, J. Solution Chem. **6**, 819 (1977).
[5] W. Ebeling and M. Grigo, J. Solution Chem. **11**, 151 (1982).
[6] M. E. Fisher and Y. Levin, Phys. Rev. Lett. **71**, 3826 (1993).
[7] Y. Levin and M. E. Fisher, Physica A **225**, 164 (1996).
[8] V. Kobelev, A. B. Kolomeisky, and M. E. Fisher, J. Chem. Phys. **116**, 7589 (2002).
[9] K. S. Pitzer, J. Phys. Chem. **77**, 268 (1973).
[10] K. S. Pitzer and G. Mayorga, J. Phys. Chem. **77**, 2300 (1973).
[11] J. G. Kirkwood, Chem. Rev. **19**, 275 (1936).
[12] R. Leote de Carvalho and R. Evans, Mol. Phys. **83**, 619 (1994).
[13] P. De Gennes, P. Pincus, R. Velasco, and F. Brochard, J. Phys. **37**, 1461 (1976).
[14] M. A. Gebbie, M. Valtiner, X. Banquy, E. T. Fox, W. A. Henderson, and J. N. Israelachvili, Proc. Natl. Acad. Sci. U.S.A. **110**, 9674 (2013).
[15] A. A. Lee, C. S. Perez-Martinez, A. M. Smith, and S. Perkin, Faraday Discuss. **199**, 239 (2017).
[16] The magnetic Coulomb energy $E_C = \mu_0 Q^2/4\pi r$ may alternatively be written $E_C = q^2/4\pi\epsilon_0 r$, where q is measured in Coulombs and $Q = cq$ where c is the speed of light.
[17] V. Kaiser, Ph.D. thesis, ENS Lyon/TU Dresden, 2014.
[18] M. J. Harris, S. T. Bramwell, D. F. McMorrow, T. Zeiske, and K. W. Godfrey, Phys. Rev. Lett. **79**, 2554 (1997).
[19] S. T. Bramwell and M. J. P. Gingras, Science **294**, 1495 (2001).
[20] A. P. Ramirez, A. Hayashi, R. J. Cava, R. Siddharthan, and B. S. Shastry, Nature (London) **399**, 333 (1999).
[21] I. A. Ryzhkin, J. Exp. Theor. Phys. **101**, 481 (2005).
[22] C. Castelnovo, R. Moessner, and S. L. Sondhi, Nature (London) **451**, 42 (2008).
[23] I. A. Ryzhkin, Solid State Commun. **52**, 49 (1984).
[24] P. Fulde, K. Penc, and N. Shannon, Ann. Phys. **11**, 892 (2002).
[25] C. L. Henley, Ann. Rev. Condens. Matter Phys. **1**, 179 (2010).
[26] B. C. den Hertog and M. J. P Gingras, Phys. Rev. Lett. **84**, 3430 (2000).
[27] M. E. Brooks-Bartlett, S. T. Banks, L. D. C. Jaubert, A. Harman-Clarke, and P. C. W. Holdsworth, Phys. Rev. X **4**, 011007 (2014).
[28] A. C. Maggs and V. Rossetto, Phys. Rev. Lett. **88**, 196402 (2002).

[29] M. F. Faulkner, S. T. Bramwell, and P. C. W. Holdsworth, Phys. Rev. B **91**, 155412 (2015).

[30] C. Castelnovo, R. Moessner, and S. L. Sondhi, Phys. Rev. B **84**, 144435 (2011).

[31] H. D. Zhou, S. T. Bramwell, J. G. Cheng, C. R. Wiebe, G. Li, L. Balicas, J. A. Bloxsom, H. J. Silverstein, J. S. Zhou, J. B. Goodenough, and J. S. Gardner, Nat. Commun. **2**, 478 EP (2011).

[32] L. Pauling, J. Am. Chem. Soc. **57**, 2680 (1935).

[33] G. N. Lewis and M. Randall, J. Am. Chem. Soc. **43**, 1112 (1921).

[34] G. Möller and R. Moessner, Phys. Rev. Lett. **96**, 237202 (2006).

[35] L. D. C. Jaubert and P. C. W. Holdsworth, J. Phys.: Condens. Matter **23**, 164222 (2011).

[36] C. Castelnovo and P. C. W. Holdsworth, *Spin Ice*, edited by L. D. C. Jaubert and M. Udagawa (Springer, Berlin, 2018).

[37] D. Frenkel and B. Smit, *Understanding Molecular Simulations* (Academic, London, 2002).

[38] P. C. Guruciaga, S. A. Grigera, and R. A. Borzi, Phys. Rev. B **90**, 184423 (2014).

[39] R. Dickman and G. Stell, AIP Conf. Proc. **492**, 225 (1999).

[40] R. A. Borzi, D. Slobinsky, and S. A. Grigera, Phys. Rev. Lett. **111**, 147204 (2013).

[41] R. G. Melko and M. J. P. Gingras, J. Phys.: Condens. Matter **16**, R1277 (2004).

[42] W. F. Giauque and J. W. Stout, J. Am. Chem. Soc. **58**, 1144 (1936).

[43] C. G. Salzmann, P. G. Radaelli, B. Slater, and J. L. Finney, Phys. Chem. Chem. Phys. **13**, 18468 (2011).

[44] D. Pomaranski, L. R. Yaraskavitch, S. Meng, K. A. Ross, H. M. L. Noad, H. A. Dabkowska, B. D. Gaulin, and J. B. Kycia, Nat. Phys. **9**, 353 (2013).

[45] V. Kaiser, S. T. Bramwell, P. C. W. Holdsworth, and R. Moessner, Nat. Mater. **12**, 1033 (2013).

[46] L Savary and L Balents, Phys. Rev. Lett. **108**, 037202 (2012).

[47] L. D. C. Jaubert, M. J. Harris, T. Fennell, R. G. Melko, S. T. Bramwell, and P. C. W. Holdsworth, Phys. Rev. X **3**, 011014 (2013).

[48] Y. Levin, Rep. Prog. Phys. **65**, 1577 (2002).

[49] E. A. Guggenheim, Trans. Faraday Soc. **55**, 1714 (1959).

[50] W. Ebeling, S. Hilbert, and H. Krienke, J. Mol. Liq. Phys. Chem. Liq. **96–97**, 409 (2002).

[51] S. K. Das, J. Horbach, K. Binder, M. E. Fisher, and J. V. Sengers, J. Chem. Phys. **125**, 024506 (2006).

[52] J. F. Nagle, J. Math. Phys. **7**, 1484 (1966).

[53] S. V. Isakov, K. S. Raman, R. Moessner, and S. L. Sondhi, Phys. Rev. B **70**, 104418 (2004).

[54] S. T. Bramwell, M. J. Harris, B. C. den Hertog, M. J. P. Gingras, J. S. Gardner, D. F. McMorrow, A. R. Wildes, A. L. Cornelius, J. D. M. Champion, R. G. Melko, and T. Fennell, Phys. Rev. Lett. **87**, 047205 (2001).

[55] S. R. Giblin, M. Twengström, L. Bovo, M. Ruminy, M. Bartkowiak, P. Manuel, J. C. Andresen, D. Prabhakaran, G. Balakrishnan, E. Pomjakushina, C. Paulsen, E. Lhotel, L. Keller, M. Frontzek, S. C. Capelli, O. Zaharko, P. A. McClarty, S. T. Bramwell, P. Henelius, and T. Fennell, Phys. Rev. Lett. **121**, 067202 (2018).

[56] Z. Hiroi, K. Matsuhira, S. Takagi, T. Tayama, and T. Sakakibara, J. Phys. Soc. Jpn. **72**, 411 (2003).

[57] B. Klemke, M. Meissner, P. Strehlow, K. Kiefer, S. A. Grigera, and D. A. Tennant, J. Low Temp. Phys. **163**, 345 (2011).

[58] M. Ruminy, M. N. Valdez, B. Wehinger, A. Bosak, D. T. Adroja, U. Stuhr, K. Iida, K. Kamazawa, E. Pomjakushina, D. Prabakharan, M. K. Haas, L. Bovo, D. Sheptyakov, A. Cervellino, R. J. Cava, M. Kenzelmann, N. A. Spaldin, and T. Fennell, Phys. Rev. B **93**, 214308 (2016).

[59] S. T. Bramwell, Nat. Commun. **8**, 2088 (2017).

[60] A. Sen, R. Moessner, and S. L. Sondhi, Phys. Rev. Lett. **110**, 107202 (2013).

[61] T. Fennell, P. P. Deen, A. R. Wildes, K. Schmalzl, D. Prabhakaran, A. T. Boothroyd, R. J. Aldus, D. F. McMorrow, and S. T. Bramwell, Science **326**, 415 (2009).

[62] L. D. C. Jaubert and P. C. W. Holdsworth, Nat. Phys. **5**, 258 (2009).

[63] E. R. Kassner, A. B. Eyvazov, B. Pichler, T. J. S. Munsie, H. A. Dabkowska, G. M. Luke, and J. C. S. Davis, Proc. Natl. Acad. Sci. U.S.A. **112**, 8549 (2015).

[64] L. Bovo, X. Moya, D. Prabhakaran, Y.-A. Soh, A. T. Boothroyd, N. D. Mathur, G. Aeppli, and S. T. Bramwell, Nat. Commun. **5**, 3439 (2014).

[65] L. D. C. Jaubert, T. Lin, T. S. Opel, P. C. W. Holdsworth, and M. J. P. Gingras, Phys. Rev. Lett. **118**, 207206 (2017).

[66] H. D. Zhou, J. G. Cheng, A. M. Hallas, C. R. Wiebe, G. Li, L. Balicas, J. S. Zhou, J. B. Goodenough, J. S. Gardner, and E. S. Choi, Phys. Rev. Lett. **108**, 207206 (2012).

[67] E. A. Guggenheim, *Thermodynamics* (North-Holland, Amsterdam, 1967).

[68] E. Lantagne-Hurtubise, J. G. Rau, and M. J. P. Gingras, Phys. Rev. X **8**, 021053 (2018).

[69] R. Evans and T. Sluckin, Mol. Phys. **40**, 413 (1980).

[70] R. R. Netz, Eur. Phys. J. E **5**, 557 (2001).

[71] C. Merlet, B. Rotenberg, P. A. Madden, P.-L. Taberna, P. Simon, Y. Gogotsi, and M. Salanne, Nat. Mater. **11**, 306 (2012).

[72] J. Comtet, A. Nigus, V. Kaiser, B. Coasne, L. Bocquet, and A. Siria, Nat. Mater. **16**, 634 (2017).

[73] V. Buch, A. Milet, R. Vacha, P. Jungwirth, and J. P. Devlin, Proc. Natl. Acad. Sci. U.S.A. **104**, 7342 (2007).

[74] I. A. Ryzhkin and M. I. Ryzhkin, JETP Lett. **93**, 384 (2011).

[75] R. Ludwig, Angew. Chem., Int. Ed. **40**, 1808 (2001).

[76] M. G. Sceats, J. Chem. Phys. **70**, 3927 (1979).

[77] A. H. Castro Neto, P. Pujol, and E. Fradkin, Phys. Rev. B **74**, 024302 (2006).

[78] V. G. Artemov, A. A. Volkov, N. N. Sysoev, and A. A. Volkov, Europhys. Lett. **109**, 26002 (2015).

[79] D. C. Elton, Phys. Chem. Chem. Phys. **19**, 18739 (2017).

[80] V. Kaiser, S. T. Bramwell, P. C. W. Holdsworth, and R. Moessner, Phys. Rev. Lett. **115**, 037201 (2015).

[81] C. Paulsen, S. R. Giblin, E. Lhotel, D. Prabhakaran, G. Balakrishnan, K. Matsuhira, and S. T. Bramwell, Nat. Phys. **12**, 661 (2016).

[82] A. Sen and R. Moessner, Phys. Rev. Lett. **114**, 247207 (2015).

[83] Roger G. Melko, B. C. den Hertog, and Michel J. P. Gingras, Phys. Rev. Lett. **87**, 067203 (2001).

[84] T. Yavors'kii, T. Fennell, M. J. P. Gingras, and S. T. Bramwell, Phys. Rev. Lett. **101**, 037204 (2008).

[85] L. D. C. Jaubert, M. Haque, and R. Moessner, Phys. Rev. Lett. **107**, 177202 (2011).

[86] J. F. Nagle, Phys. Rev. **152**, 190 (1966).